PHYSICAL REVIEW D **96,** 094013 (2017)

Color dipole picture at low-x DIS: The mass range of active photon fluctuations

Masaaki Kuroda[*]
Center for Liberal Arts, Meijigakuin University, 244-8539 Yokohama, Japan

Dieter Schildknecht[†]
Fakultät für Physik, Universität Bielefeld, Universitätsstraße 25, D-33615 Bielefeld, Germany and Max-Planck-Institut für Physik (Werner-Heisenberg-Institut), Föhringer Ring 6, D-80805 München, Germany

(Received 11 April 2017; published 16 November 2017)

We investigate the mass range of the quark-antiquark fluctuations of the photon that are active in producing the total photoabsorption cross section in the color dipole picture, emphasizing the notions of color transparency and saturation. We consider the implications of measurements at future extensions of the available electron-proton-scattering energy.

DOI: 10.1103/PhysRevD.96.094013

I. INTRODUCTION

Deep inelastic scattering (DIS) of electrons on protons at low values of the Bjorken variable $x \equiv x_{bj} \cong Q^2/W^2 \lesssim 0.1$ (where Q^2 refers to the photon virtuality and W to the photon-proton center-of-mass energy) is a two-step process: transition, or fluctuation in modern jargon, of the photon into on-shell quark-antiquark $(q\bar{q})$ states, $\gamma^* \to q\bar{q}$, of mass $M_{q\bar{q}}$, and subsequent scattering of these states on the proton. In terms of the photon-proton (virtual) forward Compton scattering amplitude, the $q\bar{q}$ states interact with the proton via (color) gauge-invariant two-gluon exchange: the color dipole picture (CDP).[1] A model-independent analysis[2] [1] shows that the photoabsorption cross section, $\sigma_{\gamma^* p}(W^2, Q^2)$, depends on the low-$x$ scaling variable $\eta(W^2, Q^2) = (Q^2 + m_0^2)/\Lambda^2_{\rm sat}(W^2)$ [3] via $\sigma_{\gamma^* p}(W^2, Q^2) = \sigma_{\gamma^* p}(\eta(W^2, Q^2)) \sim 1/\eta(W^2, Q^2)$ for $\eta(W^2, Q^2) \gtrsim 1$ ("color transparency"), while $\sigma_{\gamma^* p}(W^2, Q^2) = \sigma_{\gamma^* p}(\eta(W^2, Q^2)) \sim \ln(1/\eta(W^2, Q^2))$ ("saturation") for $\eta(W^2, Q^2) \lesssim 1$[3] The "saturation scale" $\Lambda^2_{sat}(W^2)$ increases with a small power of W^2, and m_0 is a constant mass, in the case of light quarks somewhat below the ρ^0-meson mass. Any specific parameter-dependent ansatz [1–3] for the $q\bar{q}$-dipole-proton cross section has to interpolate between the $1/\eta(W^2, Q^2)$ and the $\ln(1/\eta(W^2, Q^2))$ dependence.

The validity of the CDP rests on the condition that in the $\gamma^* \to q\bar{q}$ transition the proton-rest-frame energy imbalance ΔE between the photon of virtuality $q^2 \equiv -Q^2 \leq 0$ and the $q\bar{q}$ state of invariant mass squared $M^2_{q\bar{q}} > 0$ be small for sufficiently large $W^2 \gg M_p^2,\ Q^2$,

$$\Delta E \simeq \frac{Q^2 + M^2_{q\bar{q}}}{W^2} M_p \ll M_p, \tag{1.1}$$

or

$$\frac{Q^2 + M^2_{q\bar{q}}}{W^2} \ll 1. \tag{1.2}$$

Compare Appendix A. The condition (1.2)

(i) restricts the kinematical range of the CDP to $x \cong Q^2/W^2 \ll 1$, and it

(ii) contains the dynamical restriction of $M^2_{q\bar{q}}/W^2 \ll 1$ from generalized vector dominance (GVD). The transition of the photon, $\gamma^* \to q\bar{q}$, to a finite range of masses, $M_{q\bar{q}}$, saturates the γ^*-proton cross section for given photon virtuality Q^2 and energy W with $x \cong Q^2/W^2 \lesssim 0.1$.

It is the purpose of this paper to present a detailed investigation of the mass range of $\gamma^* \to q\bar{q}$ fluctuations responsible for, or actively producing, the photoabsorption cross section at different values of the kinematic variables W^2, Q^2 and $\eta(W^2, Q^2)$. We emphasize the different regions of $\eta(W^2, Q^2)$ related to color transparency and saturation. We comment on the impact of a future extension of the electron-proton-scattering energy range, and on the determination of the asymptotic energy dependence of $(Q^2 = 0)$ photoproduction from the measured W-dependence of the dipole cross section.

[*]kurodam@law.meijigakuin.ac.jp
[†]schild@physik.uni-bielefeld.de

[1]Compare Refs. [1,2] for an extensive list of references.

[2]Model-independent means that the results for the photoabsorption cross section do not depend on a parameter-dependent explicit ansatz for the $q\bar{q}$-dipole-proton interaction, except for a decent unitarity-preserving high-energy behavior.

[3]The behavior in terms of $1/\eta(W^2, Q^2)$ is valid except for a logarithmic, $\ln W^2$, energy dependence of the dipole cross section $\sigma_{(q\bar{q})p}(W^2)$. See the discussion on the relation of the dipole cross section to $(Q^2 = 0)$ photoproduction to be given in Sec. IV.

II. THE PHOTOABSORPTION CROSS SECTION

We start by a discussion of the results for the photoabsorption cross section, $\sigma_{\gamma^* p}(W^2, Q^2)$, in the CDP that are shown in Fig. 1, reproduced from Ref. [2]. The results are obtained from the explicit analytic expression for $\sigma_{\gamma^* p}(W^2, Q^2)$,[4] [2]

$$\begin{aligned}\sigma_{\gamma^* p}(W^2, Q^2) &= \sigma_{\gamma_L^* p}(W^2, Q^2) + \sigma_{\gamma_T^* p}(W^2, Q^2) \\ &= \frac{\alpha R_{e^+e^-}}{3\pi}\sigma^{(\infty)}(W^2) \\ &\quad \times \left(I_T^{(1)}\left(\frac{\eta}{\rho}, \frac{\mu}{\rho}\right) G_T(u) + I_L^{(1)}(\eta, \mu) G_L(u)\right),\end{aligned} \tag{2.1}$$

derived from an ansatz for the W-dependent dipole cross section[5] that essentially, via coupling of the quark-antiquark state to two gluons, comprises the color-gauge-invariant interaction of the $q\bar{q}$ dipole with the gluon field in the nucleon. In (2.1), $R_{e^+e^-} = 3\sum_q Q_q^2$, where q runs over the active quark flavors, and Q_q denotes the quark charge. The smooth transition to $Q^2 = 0$ photoproduction in (2.1) allows one [2] to replace $\sigma^{(\infty)}(W^2)$, which stems from the normalization of the dipole cross section, by the photoproduction cross section, i.e.

$$\begin{aligned}\sigma_{\gamma^* p}(W^2, Q^2) &= \frac{\sigma_{\gamma p}(W^2)}{\lim_{\eta \to \mu(W^2)} I_T^{(1)}\left(\frac{\eta}{\rho}, \frac{\mu(W^2)}{\rho}\right)} \\ &\quad \times \left(I_T^{(1)}\left(\frac{\eta}{\rho}, \frac{\mu}{\rho}\right) G_T(u) + I_L^{(1)}(\eta, \mu) G_L(u)\right).\end{aligned} \tag{2.2}$$

We note that $I_L^{(1)}(\eta, \mu)$ vanishes in the photoproduction $Q^2 = 0$ limit of $\eta(W^2, Q^2 = 0) = m_0^2/\Lambda_{\rm sat}^2(W^2) \equiv \mu(W^2)$, and $G_T(u \equiv \frac{\xi}{\eta}) \simeq 1$, and for later reference we also note

$$\lim_{\eta \to \mu(W^2)} I_T^{(1)}\left(\frac{\eta}{\rho}, \frac{\mu(W^2)}{\rho}\right) = \ln\frac{\rho}{\mu(W^2)}. \tag{2.3}$$

The general explicit analytic expressions for the functions $I_T^{(1)}(\frac{\eta}{\rho}, \frac{\mu(W^2)}{\rho})$ and $I_L^{(1)}(\eta, \mu)$ are not needed for the ensuing discussions, and we refer to Ref. [2], while $G_T(u \equiv \frac{\xi}{\eta})$ and $G_L(u \equiv \frac{\xi}{\eta})$ are given in (2.9) and (2.10) below. The numerical results for the photoabsorption cross section in Fig. 1 are obtained by numerical evaluation of (2.2) upon insertion of a $(\ln(W^2))^2$ fit to the experimental results for the photoproduction cross section $\sigma_{\gamma p}(W^2)$ from the Particle Data Group [4]. The results in Fig. 1 were obtained for $W = 275$ GeV. Compare Sec. IV, and Fig. 2 in Sec. IV, for the (weak) W dependence of $\sigma_{\gamma^* p}(\eta(W^2, Q^2), W^2)$ due to $\sigma^{(\infty)}(W^2)$ in (2.1) and $\sigma_{\gamma p}(W^2)$ in (2.2).

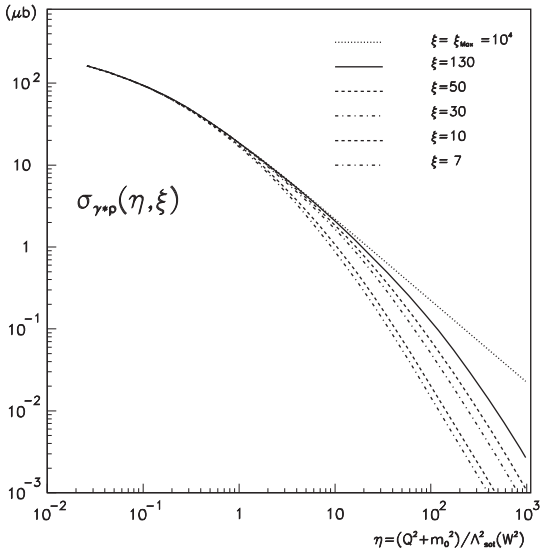

FIG. 1. The theoretical results for the photoabsorption cross section $\sigma_{\gamma^* p}(\eta(W^2, Q^2), \xi)$ in the CDP as a function of the low-x scaling variable $\eta(W^2, Q^2) = (Q^2 + m_0^2)/\Lambda_{\rm sat}^2(W^2)$ for different values of the parameter ξ that determines the (squared) mass range $M_{q\bar{q}}^2 \leq m_1^2(W^2) = \xi\Lambda_{\rm sat}^2(W^2)$ of the $\gamma^* \to q\bar{q}$ fluctuations that are taken into account. The experimental results [5] for $\sigma_{\gamma^* p}(\eta(W^2, Q^2))$ lie on the full line corresponding to $\xi = \xi_0 = 130$; compare Refs. [1,2].

Before going into more detail, we note that the full curve in Fig. 1, which for the parameter ξ corresponds to the choice of $\xi = \xi_0 = 130$, is consistent with and provides a representation of the full set of experimental data on $\sigma_{\gamma^* p}(W^2, Q^2)$; compare Fig. 9 in Ref. [1].

In (2.1) and (2.2), the low-x scaling variable $\eta(W^2, Q^2)$ is given by [3]

$$\eta \equiv \eta(W^2, Q^2) = \frac{Q^2 + m_0^2}{\Lambda_{\rm sat}^2(W^2)}, \tag{2.4}$$

with

$$\mu \equiv \mu(W^2) = \eta(W^2, Q^2 = 0) = \frac{m_0^2}{\Lambda_{\rm sat}^2(W^2)}, \tag{2.5}$$

the saturation scale, $\Lambda_{\rm sat}^2(W^2)$, being parametrized by

[4]To indicate the dependence of $\sigma_{\gamma^* p}(W^2, Q^2)$ on ξ, we frequently use, as in Fig. 1, the notation $\sigma_{\gamma^* p}(W^2, Q^2) \equiv \sigma_{\gamma^* p}(W^2, Q^2, \xi)$ as well as $\sigma_{\gamma^* p}(\eta(W^2, Q^2), \xi)$. The dependence on ξ is contained in $G_{T,L}(u \equiv \xi/\eta(W^2, Q^2))$; see (2.9) and (2.10) below.

[5]Following the suggestion of the (anonymous) referee, in Appendix B, we present a brief (critical) discussion on the approach of "geometric scaling" based on an $x \simeq Q^2/W^2$-dependent, and accordingly Q^2-dependent, ansatz for the dipole cross section.

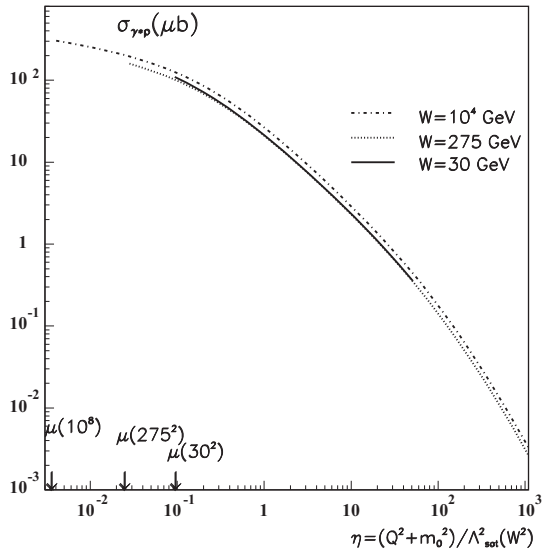

FIG. 2. The theoretical results for the photoabsorption cross section as a function of $\eta(W^2, Q^2)$ for different values of W. The dependence on W is due to logarithmic η-scaling violations $\sigma^{(\infty)}(W^2) \sim \ln W^2$; compare case (ii) in Sec. IV. For ξ the value $\xi = \xi_0 = 130$ is used, and the results for $W = 275$ GeV are identical to the results shown by the full line in Fig. 1. By definition, $\mu(W^2) \equiv m_0^2/\Lambda^2_{\rm sat}(W^2)$.

$$\Lambda^2_{\rm sat}(W^2) = C_1 \left(\frac{W^2}{1\ \text{GeV}^2}\right)^{C_2}, \tag{2.6}$$

and numerically, we have

$$m_0^2 = 0.15\ \text{GeV}^2, \quad C_1 = 0.31; \qquad C_2 = 0.27. \tag{2.7}$$

The parameter ρ is related to the longitudinal-to-transverse ratio $R(W^2, Q^2)$ of the photoabsorption cross section, and approximately we have $R(W^2, Q^2) \simeq 1/2\rho$ for $\eta(W^2, Q^2) \gg \mu(W^2)$, while $R(W^2, Q^2) = 0$ for $Q^2 = 0$. The total cross section is fairly insensitive to the value of ρ, and the evaluation presented in Fig. 1 is based [2] on $\rho = \frac{4}{3}$.

Our main concern in the rest of this section and the following one centers around the dependence of the cross section (2.2) on the constant parameter ξ that, by definition, restricts the masses of the contributing $q\bar{q}$ states via

$$M^2_{q\bar{q}} \le m_1^2(W^2) = \xi \Lambda^2_{\rm sat}(W^2). \tag{2.8}$$

The dependence on ξ in (2.1) and (2.2) is contained [2] in the functions $G_{T,L}(u \equiv \xi/\eta(W^2, Q^2))$,

$$G_T(u) = \frac{2u^3 + 3u^2 + 3u}{2(1+u)^3} \simeq \begin{cases} \frac{3}{2}\frac{\xi}{\eta}, & (\eta \gg \xi), \\ 1 - \frac{3}{2}\frac{\eta}{\xi}, & (\eta \ll \xi), \end{cases} \tag{2.9}$$

and

$$G_L(u) = \frac{2u^3 + 6u^2}{2(1+u)^3} \simeq \begin{cases} 3(\frac{\xi}{\eta})^2, & (\eta \gg \xi), \\ 1 - 3(\frac{\eta}{\xi})^2, & (\eta \ll \xi). \end{cases} \tag{2.10}$$

We turn to a more detailed qualitative discussion of the theoretical predictions in Fig. 1.

The parameter ξ is bounded by $\xi \le \xi_{\rm Max}(W^2)$, where $\xi_{\rm Max}(W^2)$ corresponds to the upper limit of $m_1^2(W^2) \cong W^2$ in (2.8); the contributing $q\bar{q}$-dipole masses cannot exceed the total available $(q\bar{q})p$ center-of-mass energy W. Accordingly, we have

$$\xi_{\rm Max} = W^2/\Lambda^2_{\rm sat}(W^2), \tag{2.11}$$

as well as

$$\frac{\eta(W^2, Q^2)}{\xi_{\rm Max}(W^2)} \cong \frac{Q^2}{W^2} \cong x_{bj}, \qquad (\text{for } Q^2 \gg m_0^2), \tag{2.12}$$

where $x_{bj} \lesssim 0.1$, and

$$G_{T,L}(\xi_{\rm Max}(W^2)/\eta(W^2, Q^2)) \cong G_{T,L}(\xi_{\rm Max}(W^2)/\eta(W^2, Q^2) \to \infty). \tag{2.13}$$

The total photoabsorption cross section (2.2) for $\xi = \xi_{\rm Max}(W^2)$ becomes

$$\sigma_{\gamma^* p}(W^2, Q^2, \xi = \xi_{\rm max}) \cong \sigma_{\gamma^* p}(\eta(W^2, Q^2), \xi \to \infty). \tag{2.14}$$

Specificaly, in Fig. 1, we have $W = 275$ GeV and $\xi_{\rm Max} \simeq 10^4 \gg \eta(W^2, Q^2)$ implying the validity of (2.14).

For $\xi = \xi_{\rm Max}$, from (2.8) with (2.11), the upper bound on $q\bar{q}$-dipole masses becomes

$$\frac{M^2_{q\bar{q}}}{W^2} \le 1. \tag{2.15}$$

The prediction for the photoabsorption cross section in Fig. 1 for $\xi = \xi_{\rm Max} = 10^4$ includes contributions from $q\bar{q}$ masses that strongly violate the fundamental condition on $\Delta E/M_p \ll 1$ in (1.2).

Turning to $\xi = \xi_0 = 130 \ll \xi_{\rm Max}$, in distinction from (2.15), we find

$$\frac{M^2_{q\bar{q}}}{W^2} \le \xi_0 \frac{\Lambda^2_{\rm sat}(W^2)}{W^2} \simeq 0.01, \tag{2.16}$$

where $W = 275$ GeV from Fig. 1 was inserted. The mass range of contributing $q\bar{q}$ states is consistent with $\Delta E/M_p \ll 1$.

The experimental results on the photoabsorption cross section agree with the theoretical prediction for $\xi = \xi_0 = 130$ in Fig. 1. The distinctive difference between the

theoretical cross section for $\xi = \xi_{\rm Max}$ and the experimentally verified one for $\xi = \xi_0 = 130$ seen for $\eta(W^2, Q^2) \gtrsim 10$ in Fig. 1 explicitly demonstrates that the $(q\bar{q})p$ interaction is due to $q\bar{q}$-dipole states that are limited in mass by $M^2_{q\bar{q}} \leq \xi_0 \Lambda^2_{\rm sat}(W^2)$. The experimental data on $\sigma_{\gamma^* p}(W^2, Q^2)$ confirm the validity of the energy imbalance for $\gamma^* \to q\bar{q}$ transition in (1.2).

We turn to the theoretical results for $\xi < \xi_0$ also shown in Fig. 1. From the difference of the cross sections for $\xi < \xi_0$ and $\xi = \xi_0 = 130$ at $\eta(W^2, Q^2) \gtrsim 1$, we conclude that high-mass $q\bar{q}$-dipole contributions are definitely necessary to yield the experimental results for the forward-Compton-scattering amplitude.

The theoretical predictions for $\sigma_{\gamma^* p}(W^2, Q^2, \xi)$ for $\xi < \xi_0$ with decreasing $\eta(W^2, Q^2)$, however, show a tendency to converge towards the results obtained for $\xi = \xi_0$. This behavior indicates that with decreasing $\eta(W^2, Q^2)$ (or decreasing Q^2 at fixed W^2), nevertheless, only $q\bar{q}$ states with decreasing mass squared $M^2_{q\bar{q}} \leq \xi \Lambda^2_{\rm sat}(W^2) < \xi_0 \Lambda^2_{\rm sat}$ are actually relevant, or active, for producing the total photoabsorption cross section.

A detailed investigation of the mass range of active $\gamma^* \to q\bar{q}$ transitions is the subject of Sec. III.

III. THE MASS RANGE OF ACTIVE $\gamma^* \to q\bar{q}$ FLUCTUATIONS

We turn to quantifying the mass range of those $q\bar{q}$ states that are responsible for the major part of the experimentally observed cross section $\sigma_{\gamma^* p}(W^2, Q^2)$ in Fig. 1. The range of contributing $q\bar{q}$ masses $m_0^2 \leq M^2_{q\bar{q}} \leq m_1^2(W^2) \leq \xi \Lambda^2_{\rm sat}(W^2)$ being determined by the parameter ξ, we search for the value of ξ that yields a (substaintial) fraction of $1 - \epsilon$, where $\epsilon = {\rm const} \ll 1$, of the photoabsorption cross section $\sigma_{\gamma^* p}(W^2, Q^2)$.

Employing the expression for $\sigma_{\gamma^* p}(W^2, Q^2)$ in (2.2) together with the approximate expressions for $G_{T,L}(u \equiv \xi/\eta(W^2, Q^2))$ in (2.9) and (2.10), we find that the dependence of $\sigma_{\gamma^* p}(W^2, Q^2)$ on $\eta(W^2, Q^2)/\xi$ for $\eta(W^2, Q^2)/\xi \ll 1$ is approximately given by the factor $1 - (3/2)\eta(W^2, Q^2)/\xi$ in (2.9), i.e. upon employing (2.14),

$$\sigma_{\gamma^* p}(W^2, Q^2, \xi) = \sigma_{\gamma^* p}(\eta(W^2, Q^2), \xi_{\rm Max}) \times \left(1 - \frac{3}{2}\frac{\eta(W^2, Q^2)}{\xi}\right). \quad (3.1)$$

The experimentally observed cross section, for $\eta(W^2, Q^2)/\xi_0 \ll 1$ is represented by evaluating (3.1) for $\xi = \xi_0 = 130$,

$$\sigma_{\gamma^* p}(W^2, Q^2, \xi_0) = \sigma_{\gamma^* p}(\eta(W^2, Q^2), \xi_{\rm Max}) \times \left(1 - \frac{3}{2}\frac{\eta(W^2, Q^2)}{\xi_0}\right). \quad (3.2)$$

A fraction of $1 - \epsilon$ of the experimentally observed cross section (3.2) accordingly is associated with a value of ξ such that $\sigma_{\gamma^* p}(W^2, Q^2, \xi)$ deviates from $\sigma_{\gamma^* p}(W^2, Q^2, \xi_0)$ by the factor $(1 - \epsilon)$,

$$\sigma_{\gamma^* p}(W^2, Q^2, \xi) = \sigma_{\gamma^* p}(W^2, Q^2, \xi_0)(1 - \epsilon). \quad (3.3)$$

Substitution of (3.1) and (3.2) into (3.3) yields

$$1 - \frac{3}{2}\frac{\eta(W^2, Q^2)}{\xi} = \left(1 - \frac{3}{2}\frac{\eta(W^2, Q^2)}{\xi_0}\right)(1 - \epsilon) \quad (3.4)$$

or

$$\xi = \frac{3}{2\epsilon}\eta(W^2, Q^2)\frac{1}{1 + \frac{3\eta(W^2, Q^2)}{2\epsilon\xi_0}(1 - \epsilon)}. \quad (3.5)$$

This is the value of ξ that, according to (3.3), for given $\eta(W^2, Q^2) \ll \xi_0$ yields a fraction of $1 - \epsilon$ of the photoabsorption cross section $\sigma_{\gamma^* p}(W^2, Q^2, \xi_0)$. For $\epsilon \to 0$, consistently, we have $\xi \to \xi_0$ in (3.5), or $m_1^2(W^2) = \xi_0 \Lambda^2_{\rm sat}(W^2)$, corresponding to the experimentally observed cross section.

For $\eta(W^2, Q^2)/\xi_0 \ll \epsilon$, we may approximate (3.5) by

$$\xi = \frac{3}{2\epsilon}\eta(W^2, Q^2), \quad (3.6)$$

and this approximation is adopted subsequently. For e.g. $\epsilon = 0.1$, from (3.6), we have $\xi = 15\eta(W^2, Q^2)$. For any given $\eta(W^2, Q^2) \ll \xi_0$, from (3.5) or (3.6), we obtain a value of ξ that for e.g. $\epsilon = 0.1$ provides 90% of the experimentally verified photoabsorption cross section.

In terms of $m_1^2(W^2) = \xi \Lambda^2_{\rm sat}(W^2)$, from (3.6), we have

$$m_0^2 \leq M^2_{q\bar{q}} \leq m_1^2 = \frac{3}{2\epsilon}\eta(W^2, Q^2)\Lambda^2_{\rm sat}(W^2) = \frac{3}{2\epsilon}(Q^2 + m_0^2). \quad (3.7)$$

For any W^2 and Q^2 with $\eta(W^2, Q^2) \ll \xi_0$, the constraint (3.7) determines the mass range of $q\bar{q}$-dipole states that are essential for the cross section in the sense of providing a fraction of magnitude $1 - \epsilon$ of the photoabsorption cross section $\sigma_{\gamma^* p}(W^2, Q^2)$. In other words, the dominant contribution to the photoabsorption cross section for fixed $\eta(W^2, Q^2) \ll \xi_0$ is due to $q\bar{q}$ states that have masses below the limit given in (3.7). The masses of these active $q\bar{q}$ states are restricted by the value of the photon virtuality Q^2 according to (3.7). A fixed value of Q^2 is uniquely associated with a fixed $q\bar{q}$-dipole-mass range.

In Table I, for the choice of $\epsilon = 0.1$, we show the results of a numerical evaluation of the upper limit m_1^2 from (3.7) for various values of $\eta(W^2, Q^2) \ll \xi_0$ and for energies in

TABLE I. The (η, W) matrix elements give the numerical values from (3.7) with $\epsilon = 0.1$ of the mass range $m_0 \le M_{qq} < m_1$ of $\gamma^* \to q\bar{q}$ transitions for fixed values of $\eta(W^2, Q^2) = (Q^2 + m_0^2)/\Lambda^2_{\rm sat}(W^2)$ and energy W. At fixed η, with increasing energy W, increasing $q\bar{q}$ masses determine the cross section. At fixed W, with decreasing $\eta(W^2, Q^2)$ smaller masses determine the cross section.

W [Gev]	30	300	10^4
$\Lambda^2_{\rm sat}(W^2)$[GeV^2]	1.95	6.75	44.8
$\eta_{\rm Min}(W^2)$	7.6×10^{-2}	2.2×10^{-2}	3.3×10^{-3}
$\eta = 1$	$Q^2 = 1.8$ GeV^2 $m_1^2 = 29$ GeV^2 $m_1 = 5.4$ GeV	$Q^2 = 6.9$ GeV^2 $m_1^2 = 101$ GeV^2 $m_1 = 10$ GeV	$Q^2 = 44.7$ GeV^2 $m_1^2 = 672$ GeV^2 $m_1 = 25$ GeV
$\eta = 0.1$	$Q^2 = 4.5 \times 10^{-2}$ $m_1^2 = 2.9$ GeV^2 $m_1 = 1.7$ GeV	$Q^2 = 0.53$ GeV^2 $m_1^2 = 10.1$ GeV^2 $m_1 = 3.2$ GeV	$Q^2 = 4.3$ GeV^2 $m_1^2 = 67$ GeV^2 $m_1 = 8.2$ GeV
$\eta = \eta_{\rm Min}$		$Q^2 = 0$ $m_1^2 = 2.25$ GeV^2 $m_1 = 1.5$ GeV	

the range of $W \lesssim 300$ GeV explored at HERA [5], and at the energy $W = 10^4$ GeV recently discussed in view of future collider projects [6]. For the saturation scale $\Lambda^2_{\rm sat}(W^2)$, and for m_0^2, we use the parameters adjusted to the experimental data from HERA for $x_{bj} \cong Q^2/W^2 \lesssim 0.1$; compare (2.7).

According to Table I, for various fixed values of $\eta(W^2, Q^2)$, with increasing W, we find the expected increase of the upper limit of the masses of relevant $q\bar{q}$ states, $M^2_{q\bar{q}} \lesssim m_1^2$. For e.g. $\eta(W^2, Q^2) = 1$, we have $M^2_{q\bar{q}} \le m_1^2 = 29$ GeV^2 at $W = 30$ GeV, and $M^2_{q\bar{q}} \le m_1^2 = 101$ GeV^2 at $W = 300$ GeV, and finally $M^2_{q\bar{q}} \le m_1^2 = 672$ GeV^2 at $W = 10^4$ GeV. With decreasing $\eta(W^2, Q^2)$ at fixed W, the decrease in Q^2 is accompanied by a decrease in m_1^2, leading to (the W-dependent value of) $M^2_{q\bar{q}} \le m_1^2 = 2.25$ GeV^2 at $\eta(W^2, Q^2) = \eta(W^2, Q^2 = 0) \equiv \eta_{\rm Min}$. It is amusing to note that the value of $m_1 = 1.5$ GeV practically coincides with the value of $m_1 = 1.4$ GeV from the 1972 GVD interpretation [7,8] of the first data on DIS from the SLAC-MIT collaboration [9].

In Table II, we present the values of the scaling variable $\eta(W^2, Q^2)$ corresponding to fixed values of Q^2 [and of m_1^2 according to (3.7) with $\epsilon = 0.1$], for different values of W chosen as in Table I. The table illustrates that an identical fixed mass range, defined by $m_0^2 \le M^2_{q\bar{q}} \le m_1^2$, is responsible for cross sections in the color transparency region and the saturation region; e.g. for $Q^2 = 2$ GeV^2 and $m_1 = 5.68$ GeV, we see the transition from $\eta = 1.1 \gtrsim 1$ at $W = 30$ GeV to $\eta = 4.8 \times 10^{-2} \ll 1$ that is reached at $W = 10^4$ GeV. As a consequence of the two-gluon color-dipole interaction, a massive $q\bar{q}$ state of mass $m_0 \le M_{q\bar{q}} \le m_1$, dependent on the energy W, either interacts with a small cross section (color transparency), $\sigma_{\gamma^* p}(W, Q^2) \sim 1/\eta(W^2, Q^2)$, or with a moderately large one (saturation), $\sigma_{\gamma^* p}(W^2, Q^2) \sim \ln(1/\eta(W^2, Q^2))$.

TABLE II. The (Q^2, W) matrix elements are the values of $\eta(W^2, Q^2) = (Q^2 + m_0^2)/\Lambda^2_{\rm sat}(W^2)$. A fixed value of Q^2 is associated with a fixed (squared) mass range, $m_0^2 \le M^2_{q\bar{q}} \le m_1^2$. With increasing energy W, for fixed Q^2 and fixed $M^2_{q\bar{q}} < m_1^2$, the transition from color transparency ($\eta \gg 1$) to saturation ($\eta \ll 1$) takes place. For $Q^2 \simeq 0$, hadronlike saturation behavior occurs for all values of W shown. With decreasing Q^2 at fixed W decreasing masses, $M^2_{q\bar{q}} < m_1^2$ determine the cross section.

W [Gev]	30	300	10^4
$\Lambda^2_{\rm sat}(W^2)$[GeV^2]	1.95	6.75	44.8
$Q^2 = 10$ GeV^2 $m_1^2 = 152$ GeV^2 $m_1 = 12.3$ GeV	5.2	1.5	2.3×10^{-1}
$Q^2 = 2$ GeV^2 $m_1^2 = 32.3$ GeV^2 $m_1 = 5.68$ GeV	1.1	3.2×10^{-1}	4.8×10^{-2}
$Q^2 = 0$ $m_1^2 = 2.25$ GeV^2 $m_1 = 1.5$ GeV	7.7×10^{-2}	2.2×10^{-2}	3.3×10^{-3}

IV. THE EXTRACTION OF THE $Q^2 = 0$ PHOTOPRODUCTION CROSS SECTION

So far in this paper, we have been concerned with the $\eta(W^2, Q^2)$ dependence of the photoabsorption cross section and its connection with the mass range of contributing $\gamma^* \to q\bar{q}$ transitions. As previously mentioned, and explicitly seen in (2.1) and (2.2), there is a deviation from a pure $\eta(W^2, Q^2)$ dependence that originates from the W^2 dependence of the dipole cross section. We recall that the results in (2.1) and (2.2) follow by specializing [1–3] the generic two-gluon-exchange form of the dipole cross section

$$\sigma_{(q\bar{q})}(\vec{r}_\perp, z(1-z), W^2) = \int d^2 l_\perp \tilde{\sigma}(\vec{l}_\perp^2, z(1-z), W^2) \times (1 - e^{-\vec{l}_\perp \cdot \vec{r}_\perp}) \quad (4.1)$$

via the ansatz

$$\tilde{\sigma}(\vec{l}_\perp^2, z(1-z), W^2) = \frac{\sigma^{(\infty)}(W^2)}{\pi} \times \delta(\vec{l}_\perp^2 - z(1-z)\Lambda_{\rm sat}^2(W^2)). \quad (4.2)$$

The connection between the normalization of the dipole cross section, $\sigma^{(\infty)}(W^2)$, which coincides with the limit of the dipole cross section for $\Lambda_{\rm sat}^2(W^2)\vec{r}_\perp^2 \to \infty$, and the $Q^2 = 0$ photoproduction cross section, $\sigma_{\gamma p}(W^2)$, is implicitly contained in (2.1) to (2.3), i.e.

$$\sigma^{(\infty)}(W^2) = \frac{3\pi}{\alpha R_{e^+e^-}} \frac{1}{\ln \frac{\Lambda_{\rm sat}^2(W^2)}{m_0^2}} \sigma_{\gamma p}(W^2), \quad (4.3)$$

or

$$\sigma_{\gamma p}(W^2) = \frac{\alpha R_{e^-e^-}}{3\pi} \sigma^{(\infty)}(W^2) \ln \frac{\Lambda_{\rm sat}^2(W^2)}{m_0^2}, \quad (4.4)$$

where we put $\rho = 1$ for simplicity. According to (4.3) and (4.4), the dipole cross section $\sigma^{(\infty)}(W^2)$ and the photoproduction cross section are uniquely related to each other. For

(i) $\sigma^{(\infty)}(W^2) = $ const., from (4.4) and (2.2) with (2.3), we have strict validity of scaling in $\eta(W^2, Q^2)$, i.e. $\sigma_{\gamma^* p}(W^2, Q^2) = \sigma_{\gamma^* p}(\eta(W^2, Q^2))$, and $\sigma_{\gamma p}(W^2) \sim \ln W^2$, while for

(ii) $\sigma^{(\infty)}(W^2) \sim \ln W^2$, we have logarithmic violation of scaling in $\eta(W^2, Q^2)$ for $\sigma_{\gamma^* p}(W^2, Q^2)$, while $\sigma_{\gamma p}(W^2) \sim (\ln W^2)^2$, and finally,

(iii) a hadronlike dipole cross section, $\sigma^{(\infty)}(W^2) \sim (\ln W^2)^2$, leads to $\sigma_{\gamma p}(W^2) \sim (\ln W^2)^3$. From a different angle, a potential dependence as $(\ln W^2)^3$ was recently considered by Mueller [10].

In Fig. 2, we show the results corresponding to case (ii), based on the high-energy extrapolation in W of the fit to photoproduction experimental data based on assuming hadronlike behavior, $\sigma_{\gamma p} \sim (\ln W^2)^2$ [4]. We recall that a dependence as $(\ln W^2)^2$ for hadron-hadron interactions was first predicted by Heisenberg [11] and later recognized as the maximally allowed growth by Froissart [12]. We note that the hadronlike behavior of photoproduction assumed in Fig. 2 is associated with a $\ln W^2$ behavior of the dipole cross section $\sigma^{(\infty)}(W^2)$, and not with the hadronlike $(\ln W^2)^2$ behavior corresponding to case (iii).

The important conclusion from the above discussion is obvious. The measurement of $\sigma_{\gamma^* p}(W^2, Q^2)$ at fixed $\eta(W^2, Q^2)$ as a function of W^2 allows one to extract $\sigma^{(\infty)}(W^2)$, and, according to (4.4), allows one to extract the $Q^2 = 0$ photoproduction cross section. Compare Fig. 2, which illustrates the specific case (ii) of $\sigma_{\gamma p}(W^2) \sim (\ln W^2)^2$.

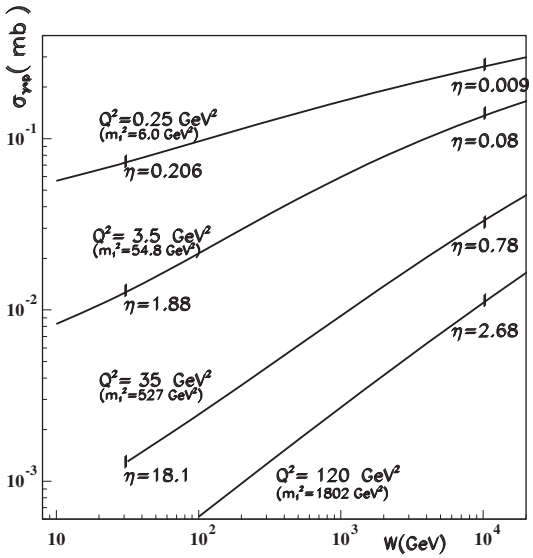

FIG. 3. The photoabsorption cross section as a function of the energy W for different values of Q^2. Note that a fixed value of Q^2 is associated with a fixed mass range of $q\bar{q}$ dipole states, $M_{q\bar{q}}^2 \leq m_1^2$ as determined by (3.7). Compare also Table II. Transition from color transparency to saturation at fixed Q^2 is a consequence of the two-gluon coupling of the $q\bar{q}$-dipole state.

In Fig. 3, we show the photoabsorption cross section for fixed values of $Q^2 > 0$ as a function of W reaching $W \cong 10^4$ GeV, the energy range discussed in connection with future electron-proton colliders [6]. As indicated in Fig. 3, fixed values of Q^2, according to (3.7), correspond to definite fixed values of $m_0^2 \leq M_{q\bar{q}}^2 \leq m_1^2$. The approach to the true asymptotic limit [2,3] of

$$\lim_{\substack{W\to\infty \\ Q_1^2, Q_2^2 > 0 \text{ fixed}}} \frac{\sigma_{\gamma^* p}(W^2, Q_1^2)}{\sigma_{\gamma^* p}(W^2, Q_2^2)} = 1, \quad (4.5)$$

or

$$\lim_{\substack{W\to\infty \\ Q^2 > 0 \text{ fixed}}} \frac{\sigma_{\gamma^* p}(W^2, Q^2)}{\sigma_{\gamma p}(W^2)} = 1, \quad (4.6)$$

according to Fig. 3 is extremely slow. Empirical evidence for the behavior in (4.5) and (4.6) can nevertheless be obtained from precise measurements at values of Q^2 around $Q^2 \cong 1$ GeV^2.

V. CONCLUSIONS

The present work is concerned with an interpretation of the photoabsorption cross section in terms of the range of the masses $M_{q\bar{q}}$ of $\gamma^* \to q\bar{q}$-dipole states that actively contribute to this cross section. The essential result is contained in (3.7). The mass range of active $q\bar{q}$ fluctuations is uniquely determined by a proportionality to the photon virtuality Q^2. At fixed $Q^2 \geq 0$, it is a fixed range of dipole masses that, as a consequence of the two-gluon $q\bar{q}$ dipole coupling, with sufficient increase of the energy W leads to the observed transition from color transparency, $\sigma_{\gamma^* p}(\eta(W^2, Q^2)) \sim 1/\eta(W^2, Q^2)$ for $\eta(W^2, Q^2) \gg 1$, to saturation, $\sigma_{\gamma^* p}(\eta(W^2, Q^2)) \sim \ln(1/\eta(W^2, Q^2))$ for $\eta(W^2, Q^2) \ll 1$. Alternatively, at fixed energy W, a sufficient decrease in Q^2 towards $Q^2 \cong 0$, associated with a decrease of the mass range of active fluctuations, also leads from $\eta(W^2, Q^2) \gg 1$ (color transparency) to $\eta(W^2, Q^2) \ll 1$ (saturation). Even though for $Q^2 > 0$ fixed, the active $q\bar{q}$ fluctuations have a larger mass than at $Q^2 = 0$, in the true limit of $W \to \infty$ the ratio of the cross section at fixed $Q^2 > 0$, to the $Q^2 = 0$ photoproduction cross section converges towards unity.

The low-x scaling of the photoabsorption cross section in $\eta(W^2, Q^2)$ is weakly violated by a $\ln W^2$ dependence due to the dipole cross section, $\sigma^{(\infty)}(W^2)$. The extraction of the W-dependence of the dipole cross section from DIS electron-proton scattering allows one to determine the $Q^2 = 0$ photoproduction cross section and to verify or falsify a hadronlike $(\ln W^2)^2$ dependence.

APPENDIX A: THE ENERGY IMBALANCE ΔE

To make this paper self-confined, we add a discussion on the energy imbalance ΔE in (1.1).

Consider the transition of the (virtual spacelike) photon of virtuality $q^2 = (q^0)^2 - \vec{q}^2 = -Q^2 \leq 0$ to a $q\bar{q}$ state of four-momentum K^μ with $K^2 \equiv K^\mu K_\mu = (K^0)^2 - \vec{K}^2 > 0$. With equality of the three-momenta of the photon and the $q\bar{q}$ state, $\vec{K} = \vec{q}$, the energy imbalance ΔE is given by

$$\Delta E = K^0 - q^0 = \frac{(K^0)^2 - (q^0)^2}{K^0 + q^0} = \frac{Q^2 + K^2}{K^0 + q^0}. \tag{A1}$$

We have to consider the high-energy limit of $q^0 = |\vec{q}|\sqrt{1 - \frac{Q^2}{\vec{q}^2}} \cong |\vec{q}|$ and $K^0 = |\vec{K}|\sqrt{1 + \frac{K^2}{\vec{K}^2}} \cong |\vec{K}| = |\vec{q}|$, where

$$\begin{aligned} \vec{q}^2 &\gg Q^2, \\ \vec{q}^2 = \vec{K}^2 &\gg K^2, \end{aligned} \tag{A2}$$

and obtain

$$\Delta E \simeq \frac{Q^2 + K^2}{2|\vec{q}|}. \tag{A3}$$

To treat the interaction of the photon with the proton of four-momentum p_μ and mass M_p, it is essential to introduce the center-of-mass energy squared, $W^2 = (p + q)^2 = M_p^2 + 2M_p q^0 - Q^2$, and $q^0 \equiv \nu$ in the proton rest frame, and $x_{bj} \equiv \frac{Q^2}{2M_p \nu} \ll 1$, and accordingly also $W^2 \simeq 2M_p \nu$. The energy imbalance (A2) becomes

$$\Delta E \simeq \frac{Q^2 + K^2}{W^2} M_p. \tag{A4}$$

It coincides with (1.1), since $M_{q\bar{q}}^2 = K^2$, to the explicit representation of which we turn now.

The four-momenta of the quark and the antiquark are denoted by $k = (k^0, \vec{k})$ and $k' = (k'^0, \vec{k}')$, where $k^2 = k'^2 = m_q^2$, and, without much loss of generality, we assume massless quarks, $m_q = 0$. We choose the z-axis of a coordinate system in the direction of the three-momentum $\vec{q} = \vec{k} + \vec{k}'$. For the ensuing discussion of the high-energy limit (A2), it is useful to represent the quark and antiquark momenta as

$$\begin{aligned} \vec{k} &= z\vec{q} + \vec{k}_\perp, \\ \vec{k}' &= (1 - z)\vec{q} - \vec{k}_\perp, \end{aligned} \tag{A5}$$

where $\vec{k}_\perp \cdot \vec{q} = 0$. The mass squared of the $q\bar{q}$ state, $M_{q\bar{q}}^2$, is given by

$$\begin{aligned} M_{q\bar{q}}^2 = K^2 &= (k^0 + k'^0)^2 - (\vec{k} + \vec{k}')^2 \\ &= 2\sqrt{(z(1 - z)\vec{q}^2 - \vec{k}_\perp^2)^2 + \vec{q}^2 \vec{k}_\perp^2} \\ &\quad - 2(z(1 - z)\vec{q}^2 - \vec{k}_\perp^2) \\ &= 2\sqrt{(k_z k'_z - \vec{k}_\perp^2)^2 + (k_z + k'_z)^2 \vec{k}_\perp^2} \\ &\quad - 2(k_z k'_z - \vec{k}_\perp^2), \end{aligned} \tag{A6}$$

where $k_z \equiv z|\vec{q}|$ and $k'_z \equiv (1 - z)|\vec{q}|$ were introduced in the last equality in (A6). One may check, as we did, that (A6) is (trivially) reproduced by applying a Lorentz transformation of magnitude $|\vec{q}|$ in the z direction to the $q\bar{q}$ state at rest.

The relation (1.1) on ΔE requires finiteness of K^2 in the high-energy limit of $z(1 - z)\vec{q}^2 \gg \vec{k}_\perp^2$, implying a necessary cancellation among the $z(1 - z)\vec{q}^2$ terms in (A6). The cancellation occurs if and only if $|z(1 - z)| = z(1 - z)$, or $z(1 - z) > 0$ or $0 < z < 1$. Expansion of the square root in (A6) for $z(1 - z)\vec{q}^2 \gg \vec{k}_\perp^2$ yields

$$M^2_{q\bar{q}} = K^2 \simeq 2(z(1-z)\vec{q}^2 - \vec{k}^2_\perp) \times \left(1 + \frac{\vec{q}^2\vec{k}^2_\perp}{2(z(1-z)\vec{q}^2 - \vec{k}^2_\perp)^2}\right) - 2(z(1-z)\vec{q}^2 - \vec{k}^2_\perp), \tag{A7}$$

or

$$M^2_{q\bar{q}} = K^2 \simeq \frac{\vec{k}^2_\perp}{z(1-z)}\left(1 + \frac{\vec{k}^2_\perp}{z(1-z)\vec{q}^2}\right) \simeq \frac{\vec{k}^2_\perp}{z(1-z)}. \tag{A8}$$

We add the comment that upon solving the equation in (A6) for $\vec{k}^2_\perp/z(1-z)$ in terms of K^2, $\vec{q}^2$ and $z(1-z)$, one finds

$$\frac{\vec{k}^2_\perp}{z(1-z)} = \frac{K^2}{1+\frac{K^2}{\vec{q}^2}}\left(1 + \frac{K^2}{4z(1-z)\vec{q}^2}\right). \tag{A9}$$

Requiring $z(1-z)\vec{q}^2 \gg K^2$ reproduces the result (A8).

From (A9), upon introducing $\sin^2\vartheta_{cm}$, where ϑ_{cm} denotes the polar angle of the quark in the $q\bar{q}$ center-of-mass frame,

$$\sin^2\vartheta_{cm} = \frac{\vec{k}^2_\perp}{\vec{k}^2_{cm}} = \frac{4\vec{k}^2_\perp}{K^2}, \tag{A10}$$

we find

$$\sin^2\vartheta_{cm} = \frac{4k^2_\perp}{K^2} = \frac{4z(1-z) + \frac{K^2}{|\vec{q}|^2}}{1+\frac{K^2}{\vec{q}^2}} \cong 4z(1-z). \tag{A11}$$

Combining (A10) and (A8) yields

$$M^2_{q\bar{q}} = K^2 = \frac{4\vec{k}^2_\perp}{\sin^2\vartheta_{cm}} \cong \frac{\vec{k}^2_\perp}{z(1-z)}. \tag{A12}$$

The fraction z of the momentum $\vec{q}$ of the photon taken over by the quark, or rather the product $z(1-z)$, in the $\vec{q} \to \infty$ limit yields the sine of the polar angle ϑ_{vm}.

In the CDP, we are exclusively dealing with the $\vec{q}^2 \to \infty$ limit, and accordingly we replace the approximate equalities in (A8) and (A12) by the equality

$$M^2_{q\bar{q}} = K^2 = \frac{4k^2_\perp}{\sin^2\vartheta_{cm}} = \frac{\vec{k}^2_\perp}{z(1-z)}. \tag{A13}$$

This expression for the $q\bar{q}$ mass squared enters (1.1) and (1.2) and all the subsequent considerations; $M^2_{q\bar{q}}$ denotes the square of the $q\bar{q}$ mass in the $\gamma^* \to q\bar{q}$ transition to a $q\bar{q}$ state with lifetime of order $1/\Delta E$.

APPENDIX B: COMMENT ON SATURATION AND GEOMETRIC SCALING

The representation of the experimental data in Fig. 1 for $\xi = \xi_0 = 130$ in terms of the low-x scaling variable $\eta(W^2, Q^2) = (Q^2 + m_0^2)/\Lambda^2_{\rm sat}(W^2)$ looks similar to a plot of the experimental data known as geometric scaling [13]. The result in [13] is a consequence of a "saturation model" [14] using an ansatz for the dipole cross section in the color dipole approach, $\hat{\sigma}(x, r) = \sigma_0 g(r/R_0(x))$, that depends on Bjorken $x \cong Q^2/W^2$, and, accordingly, at any given energy W the dipole cross section depends on Q^2, in strong disagreement with the very foundation of the color dipole approach. The CDP rests on the transition of the photon of spacelike virtuality, $q^2 = -Q^2 < 0$, to massive $q\bar{q}$ states of timelike mass squared, $M^2_{q\bar{q}} > 0$, associated with an energy imbalance ΔE explicitly given in (1.1). The interaction of the color-dipole-state of mass $M_{q\bar{q}}$ with the gluon field in the proton depends on the $(q\bar{q})p$ center-of-mass energy W [3,7,15], in no way different from e.g. πp or $\rho^0 p$ interaction at asymptotic energies, and it cannot depend on the photon virtuality Q^2. It must be concluded that the approach of the saturation model including its consequence of geometric scaling, even though leading to a successful fit to the experimental results, suffers from employing $x \simeq Q^2/W^2$ as argument of the dipole cross section, where W^2 should be used, and it lacks a sound theoretical justification.

Color transparency and saturation, in distinction from the saturation model, where saturation appears as an input assumption, in a consistent formulation of the CDP are recognized as a direct consequence of the two-gluon coupling of the $q\bar{q}$-dipole states. The relevance of the underlying energy imbalance ΔE between the spacelike photon of virtuality $q^2 \equiv -Q^2 < 0$ and the timelike $q\bar{q}$ states of mass squared $M^2_{q\bar{q}} > 0$, as pointed out in Sec. II in the main text, is quantitatively supported by the experimental data.

[1] M. Kuroda and D. Schildknecht, Phys. Rev. D **85**, 094001 (2012).
[2] M. Kuroda and D. Schildknecht, Int. J. Mod. Phys. A **31**, 1650157 (2016).
[3] D. Schildknecht, B. Surrow, and M. Tentyukov, Phys. Lett. B **499**, 116 (2001); G. Cvetic, D. Schildknecht, B. Surrow, and M. Tentyukov, Eur. Phys. J. C **20**, 77 (2001); D. Schildknecht, Nucl. Phys. B, Proc. Suppl. **99A**, 121 (2001); D. Schildknecht, in *Proceedings of The 9th International Workshop on Deep Inelastic Scattering, Bologna, Italy, 2001*, edited by G. Bruni *et al.* (World Scientific, Singapore, 2002), p. 798.
[4] Particle Data Group, Phys. Rev. D **86**, 1 (2012).
[5] H1 Collaboration, Eur. Phys. J. C **74**, 281 (2014); ZEUS Collaboration, Phys. Rev. D **90**, 072002 (2014).
[6] A. Caldwell and M. Wing, Eur. Phys. J. C **76**, 463 (2016).
[7] J. J. Sakurai and D. Schildknecht, Phys. Lett. **40B**, 121 (1972); B. Gorczyca and D. Schildknecht, Phys. Lett. **47B**, 71 (1973).
[8] D. Schildknecht, Acta Phys. Pol. B **37**, 595 (2006).
[9] G. Miller *et al.* (SLAC-MIT Collaboration), Phys. Rev. D **5**, 528 (1972).
[10] A. H. Mueller, in MPI für Physik, Munich, June 1–2, 2017.
[11] W. Heisenberg, *Vorträge Über Kosmische Strahlung* (Springer, Berlin, 1953), p. 155, reprinted in W. Heisenberg, *Collected Works*, Series B (Springer, Berlin, 1984), p. 498; W. Heisenberg, *Die Naturwissenschaften* 61, 1 (1974), reprinted in W. Heisenberg, *Collected Works*, Series B (Springer, Berlin, 1984), p. 912.
[12] M. Froissart, Phys. Rev. **123**, 1053 (1961).
[13] A. M. Stasto, K. J. Golec-Biernat, and J. Kwiecinski, Phys. Rev. Lett. **86**, 596 (2001).
[14] K. J. Golec-Biernat and M. Wüsthoff, Phys. Rev. D **59**, 014017 (1998).
[15] G. Cvetic, D. Schildknecht, and A. Shoshi, Eur. Phys. J. C **13**, 301 (2000); C. Everz and O. Nachtmann, Ann. Phys. (Amsterdam) **322**, 1670 (2007).